ARTICLES

Ion Size Effects on the Electrokinetic Flow in Nanoporous Membranes Caused by Concentration Gradients

Javier Cervera, Vladimir García-Morales, and Julio Pellicer*

Department of Thermodynamics, University of Valencia, E-46100 Burjasot, Spain

Received: October 11, 2002; In Final Form: May 22, 2003

The space charge model (SCM) relies on the Poisson−Boltzmann (PB) equation, and hence on the assumption of negligible ion size effects, to calculate the radial distribution of the electrical potential and ionic concentrations. The consideration of nanopores and/or high surface charge densities demands that we account for the finite ion size. In this work, the SCM has been extended by including the ion size effects in the modified PB equation, in the transport equations, and in the diffusion coefficients, through the Renkin function. The ion size effects on the electrokinetic flow through a nanoporous membrane caused by a concentration gradient under open circuit and no applied pressure gradient conditions have been analyzed. The conditions for the observation of the negative anomalous osmosis have also been studied. It has been concluded from the calculations that ion size effects decrease the average ionic concentrations in the pore solution, reduce the absolute values of the average solute flux density and the average solution velocity, and increase the absolute value of the membrane potential. Since the reduction in the solute flux density is quite significant, it is concluded that this extension of the SCM should be used, at least, when analyzing permeability measurements.

I. Introduction

Ionic transport processes across charged membranes are the basis of numerous systems of technological and biological interest. Among the variety of mathematical models that have been proposed to describe these transport processes (see ref 1 for a comprehensive review), two approaches have enjoyed a large popularity. The Teorell−Meyer−Sievers (TMS) model[2−4] considers the membrane as a homogeneous phase and requires no details on the membrane structure and the molecular-level mechanisms for ion and solvent permeation. The space charge model (SCM) developed by Osterle et al.[5−7] on the basis of previous work by Kobatake[8] and Dresner[9−11] takes into account the membrane structure to predict the transport properties. The membrane is then modeled as an array of identical, parallel cylindrical pores with electrical charge uniformly smeared over their walls. The TMS model and SCM give similar results for weakly charged membranes, but they differ considerably for strongly charged membranes. The membrane homogeneity assumed in the former overestimates the co-ion exclusion and gives incorrect results for transport magnitudes such as the solute flux and the membrane potential.[12] Thus, despite its mathematical complexity, the SCM has a large popularity.[13−22]

The SCM employs the Nernst−Planck equations to describe the flux of the ionic species, the Navier−Stokes equation to obtain the solution velocity inside the pore, and the Poisson−Boltzmann (PB) equation to calculate the radial distribution of the electrical potential and ionic concentrations. It is well-known that the diffuse double layer theory can give a suitable description of these radial distributions only when the ionic concentrations are low enough. At high pore surface charge densities and ionic concentrations, unrealistic ion accumulation near the charged pore walls[23−27] casts some doubts on the model predictions. It is then mandatory to include ion size effects in the governing transport equations. These ion size effects are significant in many problems of physical chemistry and biophysics including the ion distribution in the vicinity of a planar charged surface immersed in an electrolyte solution,[28−30] the transport of ionic drugs across the paracellular pathway of cell monolayers,[31] and the modeling of ionic transport through biological ion channels, natural nanotubes where the finite ion size cannot be neglected.[32,33]

Modifications of the PB equation to incorporate the volume effect of the hydrated ions have been proposed by Bikerman,[34] Grimley and Mott,[35] Eigen and Wicke,[36] Freise,[37] Sparnaay,[38] Brodowsky and Strehlow,[39] and Levine and Bell.[40] These studies have evidenced the difficulties involved in an accurate statistical description of electrolyte solutions at high concentrations. Nevertheless, most of these modifications of the PB equation appear to be correct for moderate concentrations (of the order of 0.1 M for a 1:1 electrolyte). These studies also suggest that the ionic volume and the dielectric saturation are the main effects tending to deplete the ionic concentrations in the diffuse electrical double layer that fills the membrane pores.[40]

Following the work of Gur et al.,[41] Cwirko and Carbonell[21−23] modified the SCM to include dielectric saturation effects and hydration forces. These modifications were also analyzed in the studies by Pintauro et al.[24−26] Thus, ion size effects could be indirectly examined through the hydration terms. An attempt to include the ion size effects in a modified PB equation was

* To whom correspondence should be addressed. E-mail: Julio.Pellicer-Garcia@uv.es. Phone: +34-963543117. Fax: +34-963543385.

10.1021/jp027187w CCC: $25.00
Published on Web 07/30/2003

carried out more recently.[27] (See also the work on the electrokinetic flow in ultrafine slits by González-Tovar et al.[42] based on the hypernetted chain−mean spherical integral equation.) The present work goes one step further by including the size effects in the modified PB equation, in the diffusion coefficients,[43] and in the transport equations, as suggested in the fundamental contributions by Haase[44] and Buck.[45] For the sake of clarity, other effects such as dielectric saturation are neglected.

The number of transport studies based on the SCM that consider axial concentration gradients is rather limited,[12,14−16,21,22,46,47] and none of them includes the ion size effects in a modified, nonlinear PB equation. This work extends significantly previous treatments by analyzing the ion size effects in the SCM when a concentration gradient is present under open circuit and no applied pressure gradient conditions.

The influence of convection on the solute flux and membrane potential is also considered. Even though the membrane separates two solutions at the same pressure, there is a pressure gradient inside the membrane that has to be considered as a driving force for transport. Kobatake et al.[48] and Westermann-Clark and Christoforou[12] showed that neglecting convection has only a small effect on calculated membrane potentials. However, the finite size of the ions and solvent molecules might enhance the importance of convection as a transport mechanism. Therefore, the definition of the convection velocity and the formulation of the transport equations should be carefully considered.

Although some authors have considered nonideal effects in the SCM,[49,50] ion size effects were not included in the activity coefficients. Mafé et al. have shown that a number of "nonideal" effects such as membrane inhomogeneity, ion association to the membrane fixed charge groups, and the dissociation equilibrium of weak fixed charge groups can be described by appropriate activity coefficients in an extended Donnan formalism.[51−53] Following these analyses, activity coefficients that account for ion size effects, as well as for other types of interactions, have been defined in this work. The calculated results, however, incorporate only ion size effects in the activity coefficients.

The SCM has been used to analyze the transport properties of membrane pores with radii as small as 1.5−2.0 nm (without taking into account the ion size effects).[23,54] From the early studies of the SCM, the question of how small a pore should be for the continuum-based equations to be applicable has emerged.[14] Although molecular dynamics simulations might be more appropriate than the PB continuum approach for the length scales involved, the fact is that extensions of this approach have often proved useful,[2,25,27−30,33] especially in those cases where long-range electrostatic forces rather than atomistic-level details dominate the behavior of macroscopic observable phenomena like the membrane potential.[32]

This work is organized according to the following scheme. First, the steady-state transport equations for nonideal solutions of finite size ions are deduced from the principles of irreversible thermodynamics. Then, the ionic concentrations and electric potential profiles in the pore cross section are analyzed. The membrane potential and the solute flux are studied as functions of parameters of experimental interest, such as the concentration difference, the membrane fixed charge density, and the ratio between the ionic and the pore radii. Finally, the role of the convective solution velocity is discussed.

II. Theory

1. Description of the Transport Problem. A charged membrane separating two aqueous solutions I and II at the same temperature T and pressure $p_I = p_{II}$ but different electrical potentials $\Phi_I \neq \Phi_{II}$ and concentrations $c_I \neq c_{II}$ of the same 1:1 binary electrolyte is considered. The two ions are assumed to have the same molecular mass M and partial molar volume υ. The molecular mass and partial molar volume of the solvent molecules are denoted by M_s and υ_s, respectively. In the SCM, the membrane is modeled as an array of parallel cylindrical pores with fixed charges uniformly smeared over their walls. The pore surface is considered to be a smooth cylinder of radius a. This is then an effective value which describes the pore structure, including the size of the membrane fixed charges. The pore length L is much larger than the pore radius, so that edge effects can be neglected. The distance between pores is so large that the transport across a single pore is representative of that across the whole membrane. The validity of these simplifying assumptions is somehow justified by the good results obtained from the SCM in the past decades. A negative surface charge density $\sigma < 0$ is assumed, although positive wall charge densities could be treated similarly.

The finite size of the ions and solvent molecules might enhance the importance of convection as a transport mechanism. The transport equations should then take convection into account. Their formulation has to consider that different definitions of the convection velocity lead to transport equations in different reference frames. The velocity calculated from the Navier−Stokes equation is the barycentric velocity, and hence, this should be preferred for establishing the fundamental transport equations. For the analysis of experimental data, however, the Fick's (or mean volume) reference frame is more convenient.[44] For the sake of simplicity, it is assumed that $M/\upsilon = M_s/\upsilon_s$, which renders the barycentric and Fick's reference frames to be equal.

The aim of the transport model is to derive the relations between the flux densities of experimental interest and the applied driving forces, taking into account the membrane structure. The transport across the membrane involves three flux densities, namely, the electric current density $\langle i \rangle$, the solute flux density $\langle j \rangle$, and the solution velocity $\langle u \rangle$, where the brackets $\langle\ \rangle$ denote average values over the pore section $0 \leq r \leq a$. Similarly, there are also three driving forces involved: the gradient of the electrolyte activity, the electric field (because a membrane potential is established under open-circuit conditions due to the different ionic mobilities and the membrane fixed charge), and the osmotic pressure difference between the bathing solutions. More exactly, the third driving force is the gradient of the effective pressure P, defined as the difference between the pressure p and the osmotic pressure Π^*.

2. Activity Coefficient and Ion Size Effects. Ion size effects can be accounted for in the thermodynamic description of transport processes across membranes through an appropriate mean activity coefficient. It is proposed in this work to define the generalized mean activity coefficient as

$$\gamma^* \equiv \gamma e^{\upsilon \Pi^*/RT} \tag{1}$$

where γ is the mean activity coefficient in the absence of ion size effects, R is the gas constant, T is the absolute temperature, and $\Pi^* \equiv RTg^*\Sigma_i c_i$ is the osmotic pressure. The molar concentration c_i of ionic species i ($i = +, -$) and that of the solvent, c_s, are related through Euler's equation

$$\upsilon_s c_s + \upsilon \Sigma_i c_i = 1 \tag{2}$$

and the osmotic coefficient g^* is defined through Bjerrum's relation[55]

$$d(g^*\Sigma_i c_i) = \frac{1}{\upsilon_s c_s}[\Sigma_i c_i\, d\ln\gamma + d(\Sigma_i c_i)] = \Sigma_i c_i\, d\ln(\gamma^* c_i) \quad (3)$$

In the case of point ions, $\upsilon \to 0$, $M = \rho\upsilon \to 0$, $c_s \to 1/\upsilon_s =$ constant, and $\gamma^* \to \gamma$. The osmotic pressure is then $\Pi \equiv RTg\Sigma_i c_i$ where the osmotic coefficient g is defined through Bjerrum's relation $d(g\Sigma_i c_i) = \Sigma_i c_i\, d\ln(\gamma c_i)$.

For the sake of clarity, the only deviations from the ideal solution behavior considered in this work are those associated with the finite ion size, and therefore, the values $\gamma = g = 1$ are used in the calculations presented below. The activity and osmotic coefficients simplify then to

$$\gamma^* = e^{\upsilon\Pi^*/RT} = \frac{1}{\upsilon_s c_s} = \frac{1}{1 - \upsilon\Sigma_i c_i} \geq 1 \quad (4)$$

$$g^* = \frac{\ln\gamma^*}{1 - 1/\gamma^*} = -\frac{\ln(1 - \upsilon\Sigma_i c_i)}{\upsilon\Sigma_i c_i} \geq 1 \quad (5)$$

which obviously reduce to $\gamma^* = g^* = 1$ in the case of point ions.

3. Reference Frame and Flux Equations. The SCM was developed initially for solutions of point ions, and hence, no coupling between the ionic and solvent flux densities was introduced. In fact, the SCM model does not consider the solvent molecules (except for providing a continuous medium of permittivity ϵ in the PB equation). The modification of the SCM to incorporate ion size effects requires the derivation of the flux equations from first principles so that the effect of pressure gradients on ionic motion is correctly taken into account.

The flux densities of the ions and solvent molecules in the barycentric reference frame, ${}_u\vec{J}_i$ and ${}_u\vec{J}_s$, are related by the equation

$$M_s\, {}_u\vec{J}_s + M\Sigma_i\, {}_u\vec{J}_i = \vec{0} \quad (6)$$

The phenomenological flux equations have to be established from the dissipation function $\Psi = -{}_u\vec{J}_s\cdot\vec{\nabla}\mu_s - \Sigma_i\, {}_u\vec{J}_i\cdot\vec{\nabla}\tilde{\mu}_i$, where μ_s and $\tilde{\mu}_i$ denote the chemical potential of the solvent and the electrochemical potential of species i, respectively. It should be observed, however, that ${}_u\vec{J}_i$ and ${}_u\vec{J}_s$ are not independent due to eq 6. Similarly, the driving forces $\vec{\nabla}\tilde{\mu}_i$ and $\vec{\nabla}\mu_s$ are not independent either. By eliminating the flux density of the solvent ${}_u\vec{J}_s$, it is obtained that $\Psi = -\Sigma_i\, {}_u\vec{J}_i\cdot\vec{\nabla}\,\tilde{\mu}_i^*$, where

$$\vec{\nabla}\tilde{\mu}_i^* \equiv \vec{\nabla}\tilde{\mu}_i - \frac{M}{M_s}\vec{\nabla}\mu_s \quad (7)$$

is the (independent) driving force for the transport of species i.[44] This transformation of the dissipation function implies that transport equations need to be formulated for the ionic species only, not for the solvent.

Making use in eq 7 of the assumption $M/\upsilon = M_s/\upsilon_s$ and the expressions

$$\vec{\nabla}\tilde{\mu}_i = RT\vec{\nabla}\ln(\gamma c_i) + z_i F\vec{\nabla}\Phi + \nu\vec{\nabla}p \quad (8)$$

$$\vec{\nabla}\mu_s = \upsilon_s\vec{\nabla}(p - \Pi^*) \quad (9)$$

it is obtained that

$$\vec{\nabla}\tilde{\mu}_i^* = RT\vec{\nabla}\ln(\gamma^* c_i) + z_i F\vec{\nabla}\Phi \quad (10)$$

where F is Faraday's constant, Φ is the electric potential, z_i is the charge number of species i, and the ionic and mean activity coefficients are assumed to be equal.

Note that eqs 8 and 9 satisfy the Gibbs−Duhem equation[44]

$$c_s\vec{\nabla}\mu_s + \Sigma_i c_i\vec{\nabla}\tilde{\mu}_i = \vec{\nabla}p + F\Sigma_i z_i c_i\vec{\nabla}\Phi \quad (11)$$

The rhs term of this equation represents the force (density) acting on the solution that fills the membrane pores and also satisfies the Navier−Stokes equation

$$\eta\nabla^2\vec{u} = \vec{\nabla}p + F\Sigma_i z_i c_i\vec{\nabla}\Phi \quad (12)$$

where $\vec{u}$ is the barycentric velocity (in the laboratory reference frame).

Finally, in the Nernst−Planck approximation, the flux density of species i in the laboratory (or membrane-fixed) reference frame is given by[44,56]

$$\vec{J}_i = c_i\vec{u} + {}_u\vec{J}_i = c_i\vec{u} - \frac{D_i c_i}{RT}\vec{\nabla}\tilde{\mu}_i^* \quad (13)$$

where D_i is the diffusion coefficient of species i and $\vec{\nabla}\tilde{\mu}_i^*$ is given by eq 10.

4. Radial Equilibrium and Change of Variables. Under the assumption that the pore length L is much larger than the pore radius a, both $\vec{J}_i$ and $\vec{u}$ have axial components only, denoted by j_i and u hereafter. Furthermore, the continuity equations $\partial j_i/\partial x = 0$ and $\partial u/\partial x = 0$ imply that these magnitudes are functions of the radial position coordinate only, that is, $j_i = j_i(r)$ and $u = u(r)$.

The absence of radial components of $\vec{J}_i$ and $\vec{u}$ is represented by the equations[15,57,58]

$$\frac{\partial}{\partial r}[\ln(\gamma^* c_i) + z_i\phi] = 0 \quad (14)$$

$$\frac{\partial p}{\partial r} + F\Sigma_i z_i c_i\frac{\partial\Phi}{\partial r} = \frac{\partial(p - \Pi^*)}{\partial r} = 0 \quad (15)$$

where $\phi \equiv F\Phi/RT$ is the dimensionless electric potential. It can be shown from eq 9 that eq 15 represents not only the mechanical equilibrium of the solution in the radial direction but also the distribution equilibrium of the solvent, $\partial\mu_s/\partial r = 0$. Similarly, eq 14 implies $\partial\tilde{\mu}_i/\partial r = 0$.

Since μ_s, $\tilde{\mu}_i$, and $\tilde{\mu}_i^*$ are functions of x only, it is possible to transform eqs 12 and 13 to a system of ordinary differential equations by writing the gradients of μ_s and $\tilde{\mu}_i^*$ in terms of state variables with no radial dependence. These variables can be defined from eqs 14 and 15 as

$$C(x) \equiv \gamma^*[c_+(r,x)\, c_-(r,x)]^{1/2} \quad (16)$$

$$V(x) \equiv \phi(r,x) - \psi(r,x) \quad (17)$$

$$P(x) \equiv p(r,x) - \Pi^*(r,x) \quad (18)$$

where

$$\psi(r,x) \equiv \ln\frac{\gamma^* c_-}{C} = -\ln\frac{\gamma^* c_+}{C} \quad (19)$$

This change of variables is justified not only for the sake of mathematical simplicity but also because of its clear physical meaning. Since $\tilde{\mu}_i = \mu_i^\circ + RT\ln C + z_i RTV + \upsilon P$, where μ_i° denotes the standard chemical potential of species i, $C(x)$, $V(x)$, and $P(x)$ represent the electrolyte concentration, electrical potential, and effective pressure of an hypothetical ideal bulk solution that would be in electrochemical equilibrium with the solution at position (r,x);[7,14] some authors give P the meaning

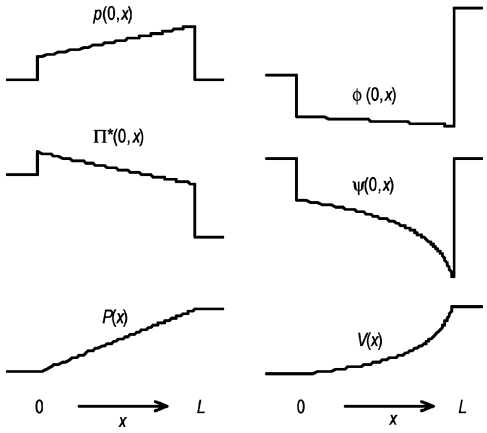

Figure 1. Schematic representation of the axial distributions of pressure p and potential ϕ and their components Π^*, P, ψ, and V for the concentration ratios $c_I/c_{II} = 5$ and $c_{II}/X = 0.1$.

of a partial pressure of the solvent.[6] This can be better understood by considering the boundary conditions at the membrane|solution interfaces. The Donnan equilibrium conditions require that μ_s and $\tilde{\mu}_i$ must be continuous across the membrane|solution interfaces at $x = 0$ and L. This implies that C, V, and P must also be continuous across the interfaces, and hence

$$C(0) = \gamma_I^* c_I = \frac{c_I}{1 - 2\upsilon c_I} \tag{20a}$$

$$C(L) = \gamma_{II}^* c_{II} = \frac{c_{II}}{1 - 2\upsilon c_{II}} \tag{20b}$$

$$V(0) = \phi_I, \quad V(L) = \phi_{II} \tag{21}$$

$$P(0) = p_I - \Pi_I^* = p_I + \frac{RT}{\upsilon}\ln(1 - 2\upsilon c_I) \tag{22a}$$

$$P(L) = p_{II} - \Pi_{II}^* = p_{II} + \frac{RT}{\upsilon}\ln(1 - 2\upsilon c_{II}) \tag{22b}$$

where $\Pi_I^* \equiv 2RTg_I^* c_I$, $\Pi_{II}^* \equiv 2RTg_{II}^* c_{II}$, and eqs 4 and 5 have been used. Equations 20a−22b implicitly assume that the standard chemical potentials of the ions and the solvent do not change significantly when crossing the membrane|solution interface; otherwise, partition coefficients would need to be included.

The decomposition of the electrical potential ϕ was first introduced by Osterle et al.[5−7] and allows for a simple solution of the nonlinear PB equation. Although some authors have noted the apparent arbitrariness of this decomposition,[25] it should be stressed that eqs 16, 17, and 19 rigorously define ψ and V. The decomposition of p and ϕ is illustrated in Figure 1, which sketches the axial distributions of p and ϕ and their components Π^*, P, ψ, and V for the concentration ratio $c_I/c_{II} = 5$ and $c_{II}/X = 0.1$. Note that while p, Π^*, ϕ, and ψ are discontinuous at the membrane|solution interfaces, P and V are continuous there. The interfacial pressure drop must then be equal to the osmotic pressure drop, $\Delta_D p = \Delta_D \Pi$, where Δ_D denotes the difference between the value on the membrane side of the interface and the value in the external solution. Analogously, since V is continuous across the interfaces, the magnitudes $\psi(r,0)$ and $\psi(r,L)$ are equivalent to the Donnan potential drops in the TMS theory. These potential drops arise because of the space charge distribution at the interfacial regions around $x = 0$ and L.[59]

5. Space Charge Distribution. The equilibrium radial distribution of space charge in the pore section accessible to the ions, $0 < r < a^* \equiv a - a_i$, where a and a_i are the pore and the ionic radii, respectively, is governed by the Poisson equationand the boundary conditions[60]

$$\frac{1}{r}\frac{\partial}{\partial r}\left(r\frac{\partial \psi}{\partial r}\right) \approx -\frac{F^2}{\epsilon RT}\Sigma_i z_i c_i = \kappa^2 \frac{\sinh\psi}{\gamma^*} \tag{23}$$

$$\left.\frac{\partial \psi}{\partial r}\right|_{r=0} = 0 \tag{24}$$

$$\left.\frac{\partial \psi}{\partial r}\right|_{r=a^*} = \frac{F\sigma}{\epsilon RT}\frac{a}{a^*} \tag{25}$$

where $\kappa(x) \equiv [2F^2C(x)/\epsilon RT]^{1/2}$ is the reciprocal Debye length and $\partial^2\phi/\partial x^2$ has been neglected because $a \ll L$. The ion size effects are accounted for by the activity coefficient γ^* in eq 23. Evaluating γ^* from eq 4, eq 19 can be written as

$$\frac{c_-}{1 - \upsilon\Sigma_i c_i}e^{-\psi} = \frac{c_+}{1 - \upsilon\Sigma_i c_i}e^{\psi} = C \tag{26}$$

which resembles the Bikerman equation.[27,28,34] However, it should be noticed that the Bikerman equation involves ϕ and not ψ, and that eq 26 merely defines ψ.

Equations 23−25 imply that electroneutrality is fulfilled over any pore section. The amount of charge fixed to the pore walls per volume of pore solution, $2\sigma/a < 0$, must be compensated by the charge density FX of the ions in the pore section

$$X = \Sigma_i z_i \langle c_i \rangle = \frac{2}{a^2}\Sigma_i z_i \int_0^{a^*} c_i r\, dr = -\frac{2\sigma}{Fa} \tag{27}$$

6. Axial Transport Equations. In terms of the variables C and V, the axial component of the Nernst−Planck equation is

$$j_i = c_i u - D_i c_i \frac{d}{dx}[\ln(\gamma^* c_i) + z_i\phi] = c_i u - D_i c_i\left(\frac{d\ln C}{dx} + z_i\frac{dV}{dx}\right) \tag{28}$$

Since dV/dx (and not $\partial\phi/\partial x$) acts as a driving force for axial transport, V is often referred to as the electromotive potential.[12]

It is very important to observe that the ion size effects described by eq 1 do not take into account the hindered diffusion of the ions across the narrow membrane pores. The activity coefficient factor $e^{\upsilon\Pi^*/RT}$ can be undestood as an equilibrium magnitude describing the coupling between solutes and solvent and indirectly establishing an upper bound for the solute concentration. In addition, transport processes through ultrafine pores are affected by the increased friction between the diffusing solutes and the pore walls, which can be accounted for through the Renkin relation[43]

$$\frac{D_i}{D_i^\circ} = 1 - 2.104\frac{a_i}{a} + 2.09\left(\frac{a_i}{a}\right)^3 - 0.95\left(\frac{a_i}{a}\right)^5 \tag{29}$$

where D_i and D_i° are the diffusion coefficients of species i inside the pore and in bulk solution. Although the Renkin relation was initially derived for neutral solutes, the transport of charged solutes is also affected by this kind of finite size effects.[31]

The axial component of the Navier−Stokes equation can be written as

$$\frac{\eta}{r}\frac{\mathrm{d}}{\mathrm{d}r}\left(r\frac{\mathrm{d}u}{\mathrm{d}r}\right)=\frac{\partial p}{\partial x}+RT\Sigma_i z_i c_i\frac{\partial \phi}{\partial x}=\frac{\mathrm{d}P}{\mathrm{d}x}+RT\left(\Sigma_i c_i\frac{\mathrm{d}\ln C}{\mathrm{d}x}+\Sigma_i z_i c_i\frac{\mathrm{d}V}{\mathrm{d}x}\right) \quad (30)$$

Integrating twice this equation, first between 0 and r and then between r and a^*, and using the nonslip condition $u = 0$ at $r = a^*$, the velocity profile is

$$u=-\frac{a^{*2}-r^2}{4\eta}\frac{\mathrm{d}P}{\mathrm{d}x}-\frac{RT}{\eta}\left(I_1\frac{\mathrm{d}\ln C}{\mathrm{d}x}+I_2\frac{\mathrm{d}V}{\mathrm{d}x}\right) \quad (31)$$

where

$$I_1(r,x)\equiv\int_r^{a^*}\frac{\mathrm{d}r'}{r'}\int_0^{r'}\Sigma_i c_i r''\,\mathrm{d}r''\equiv 2C(x)\int_r^{a^*}\frac{\mathrm{d}r'}{r'}\int_0^{r'}\frac{\cosh\psi}{\gamma^*}r''\,\mathrm{d}r'' \quad (32)$$

$$I_2(r,x)\equiv\int_r^{a^*}\frac{\mathrm{d}r'}{r'}\int_0^{r'}\Sigma_i z_i c_i r''\,\mathrm{d}r''=\frac{\epsilon RT}{F^2}[\psi(r,x)-\psi(a^*,x)] \quad (33)$$

and the Poisson equation has been used in the last equality of eq 33.

7. Solution of the Pore-Average Transport Equations. By taking average values of eqs 28 and 31 over the pore section $0 \le r \le a$,[6,7,21] the transport equations can be formulated as the following linear relations between the averaged solution velocity $\langle u\rangle$, solute flux density $\langle j\rangle \equiv \Sigma_i\langle j_i\rangle/2$, and electric current density $\langle i\rangle \equiv F\Sigma_i z_i\langle j_i\rangle$, and the three driving forces dP/dx, d ln C/dx, and dV/dx

$$-\langle u\rangle=\langle K_{uP}\rangle\frac{\mathrm{d}P}{\mathrm{d}x}+\langle K_{uC}\rangle\frac{\mathrm{d}\ln C}{\mathrm{d}x}+\langle K_{uV}\rangle\frac{\mathrm{d}V}{\mathrm{d}x} \quad (34)$$

$$-\langle j\rangle=\langle K_{jP}\rangle\frac{\mathrm{d}P}{\mathrm{d}x}+\langle K_{jC}\rangle\frac{\mathrm{d}\ln C}{\mathrm{d}x}+\langle K_{jV}\rangle\frac{\mathrm{d}V}{\mathrm{d}x} \quad (35)$$

$$-\langle i\rangle/F=\langle K_{iP}\rangle\frac{\mathrm{d}P}{\mathrm{d}x}+\langle K_{iC}\rangle\frac{\mathrm{d}\ln C}{\mathrm{d}x}+\langle K_{iV}\rangle\frac{\mathrm{d}V}{\mathrm{d}x} \quad (36)$$

where[6]

$$K_{uP}\equiv\frac{a^{*2}-r^2}{4\eta},\quad 0<r<a^* \quad (37)$$

$$K_{uC}\equiv\frac{RT}{\eta}I_1 \quad (38)$$

$$K_{uV}\equiv\frac{RT}{\eta}I_2 \quad (39)$$

$$K_{jP}\equiv\frac{1}{2}\Sigma_i c_i\frac{a^{*2}-r^2}{4\eta} \quad (40)$$

$$K_{jC}\equiv\frac{1}{2}\left[\Sigma_i D_i c_i+\frac{RT}{\eta}\Sigma_i c_i I_1\right] \quad (41)$$

$$K_{jV}\equiv\frac{1}{2}\left[\Sigma_i z_i D_i c_i+\frac{RT}{\eta}\Sigma_i c_i I_2\right] \quad (42)$$

$$K_{iP}\equiv\Sigma_i z_i c_i\frac{a^{*2}-r^2}{4\eta} \quad (43)$$

$$K_{iC}\equiv\Sigma_i z_i D_i c_i+\Sigma_i z_i c_i\frac{RT}{\eta}I_1 \quad (44)$$

$$K_{iV}\equiv\Sigma_i D_i c_i+\Sigma_i z_i c_i\frac{RT}{\eta}I_2 \quad (45)$$

The open-circuit condition $\langle i\rangle = 0$ allows us to eliminate the gradient dV/dx from eqs 34−36 and reduce the transport equations to

$$-\langle u\rangle=\langle L_{uP}\rangle\frac{\mathrm{d}P}{\mathrm{d}x}+\langle L_{uC}\rangle\frac{\mathrm{d}\ln C}{\mathrm{d}x} \quad (46)$$

$$-\langle j\rangle=\langle L_{jP}\rangle\frac{\mathrm{d}P}{\mathrm{d}x}+\langle L_{jC}\rangle\frac{\mathrm{d}\ln C}{\mathrm{d}x} \quad (47)$$

where ($\alpha = u, j$; $\beta = P, C$)

$$\langle L_{\alpha\beta}\rangle\equiv\langle K_{\alpha\beta}\rangle-\frac{\langle K_{\alpha V}\rangle\langle K_{i\beta}\rangle}{\langle K_{iV}\rangle} \quad (48)$$

Equations 46 and 47 can now be solved for the gradients to give

$$\frac{\mathrm{d}P}{\mathrm{d}x}=\frac{1}{\Delta}(-\langle L_{jC}\rangle\langle u\rangle+\langle L_{uC}\rangle\langle j\rangle) \quad (49)$$

$$\frac{\mathrm{d}\ln C}{\mathrm{d}x}=\frac{1}{\Delta}(\langle L_{jP}\rangle\langle u\rangle-\langle L_{uP}\rangle\langle j\rangle) \quad (50)$$

where $\Delta \equiv \langle L_{jC}\rangle\langle L_{uP}\rangle - \langle L_{jP}\rangle\langle L_{uC}\rangle$. By guessing initial values for $\langle j\rangle$ and $\langle u\rangle$, dP/dx and d ln C/dx can be integrated over the membrane. The values of $\langle j\rangle$ and $\langle u\rangle$ are then iteratively improved, by using a Newton−Raphson algorithm,[61] until the boundary conditions imposed on C and P are satisfied, that is, until the zeros of the functions

$$F(\langle j\rangle,\langle u\rangle)\equiv\ln\frac{\gamma_{\mathrm{I}}^* c_{\mathrm{I}}}{\gamma_{\mathrm{II}}^* c_{\mathrm{II}}}+\int_0^L\frac{\mathrm{d}\ln C}{\mathrm{d}x}\,\mathrm{d}x \quad (51)$$

$$G(\langle j\rangle,\langle u\rangle)\equiv\Pi_{\mathrm{II}}^*-\Pi_{\mathrm{I}}^*+\int_0^L\frac{\mathrm{d}P}{\mathrm{d}x}\,\mathrm{d}x \quad (52)$$

are found. (Recall that $P \equiv p - \Pi^*$ and $p_{\mathrm{I}} = p_{\mathrm{II}}$.) Finally, the membrane potential is obtained as

$$\Delta V\equiv\phi_{\mathrm{II}}-\phi_{\mathrm{I}}=V(L)-V(0)=\int_0^L\frac{\mathrm{d}V}{\mathrm{d}x}\,\mathrm{d}x \quad (53)$$

where

$$\frac{\mathrm{d}V}{\mathrm{d}x}=\frac{\Sigma_i z_i\langle c_i u\rangle}{\Sigma_i D_i\langle c_i\rangle}-\frac{\Sigma_i z_i D_i\langle c_i\rangle}{\Sigma_i D_i\langle c_i\rangle}\frac{\mathrm{d}\ln C}{\mathrm{d}x}=-\frac{\langle K_{iP}\rangle}{\langle K_{iV}\rangle}\frac{\mathrm{d}P}{\mathrm{d}x}-\frac{\langle K_{iC}\rangle}{\langle K_{iV}\rangle}\frac{\mathrm{d}\ln C}{\mathrm{d}x} \quad (54)$$

III. Results and Discussion

In this section, the variation of the solute flux density $\langle j\rangle$ and the membrane potential ΔV with the external concentration ratio $c_{\mathrm{I}}/c_{\mathrm{II}}$ and other system parameters is analyzed and discussed. In particular, the effect of the ratio of ionic to pore radii, a_i/a, is described in detail. The molar volume of the ion is calculated from the excluded volume[29,30] as $\upsilon = 8N_{\mathrm{A}}(4\pi/3)a_i^3$, where N_{A} is Avogadro's constant and a_i is the hydrated radius of species i, which is significantly larger than the crystallographic radius. Unless otherwise stated, the following values are used in the calculations: $a = 1.5$ nm, $X = 0.1$ M, $D_-^\circ = 2D_+^\circ = 2\times10^{-5}$ cm^2/s, $\eta = 1$ mPa s, $T = 300$ K, and $\epsilon = 80\epsilon_0$, where ϵ_0 is the vacuum permittivity. Whenever the effect of external solution concentration is analyzed, the concentration c_{II} is kept fixed while c_{I} is varied.

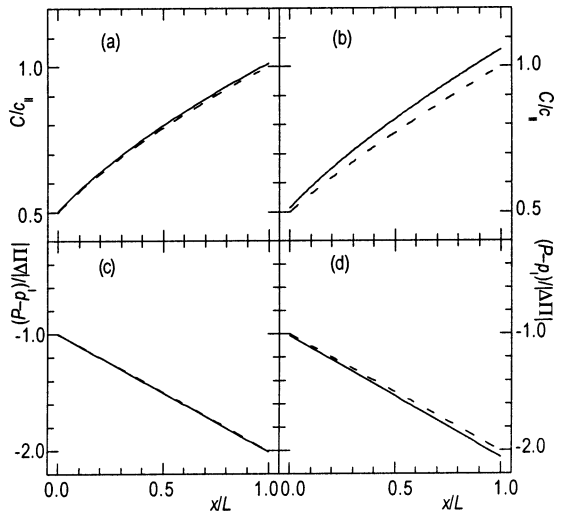

Figure 2. Axial distributions of the concentration $C(x)$ and the effective pressure $P(x)$ accross the pore length calculated for $c_{II}/X = 0.1$ (plots a and c) and 0.5 (plots b and d). The pressure P is referred to p_I and normalized to the Van't Hoff osmotic pressure difference $|\Delta\Pi| = 2RT|c_{II} - c_I|$. The concentration C is normalized to c_{II}. The external concentration ratio is $c_I/c_{II} = 0.5$. Solid curves correspond to finite-size ions of $a_i/a = 0.2$, while dashed curves correspond to point ions.

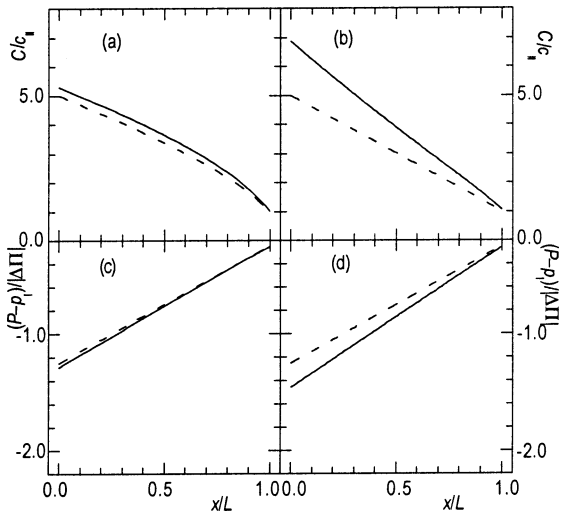

Figure 3. Axial distributions similar to those in Figure 2 for the external concentration ratio $c_I/c_{II} = 5.0$.

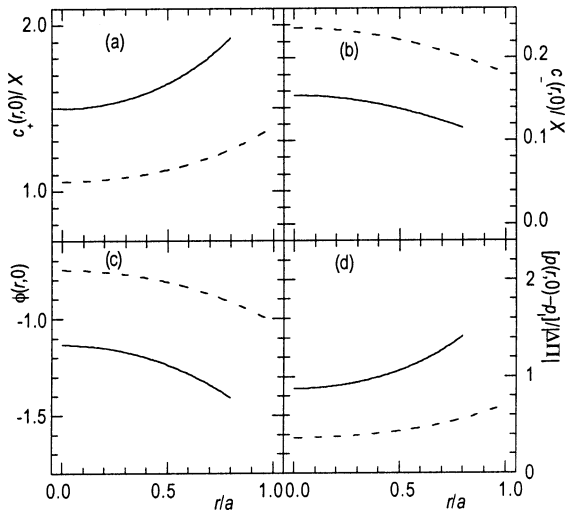

Figure 4. Radial distributions of the ionic concentrations $c_+(r,0)$ and $c_-(r,0)$, the dimensionless electric potential $\phi(r,0)$, and the pressure $p(r,0)$ at the pore end in contact with solution I for the concentration ratios $c_I/c_{II} = 5$ and $c_{II}/X = 0.1$. The pressure p is referred to p_I and normalized to the Van't Hoff osmotic pressure difference $|\Delta\Pi| = 2RT|c_{II} - c_I|$. The concentrations are normalized to X.

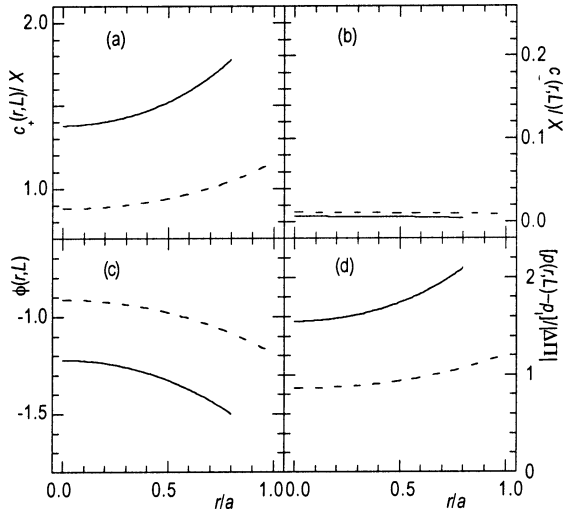

Figure 5. Radial distributions of the ionic concentrations $c_+(r,L)$ and $c_-(r,L)$, the dimensionless electric potential $\phi(r,L)$, and the pressure $p(r,L)$ at the pore end in contact with solution II calculated for the concentration ratios $c_I/c_{II} = 5$ and $c_{II}/X = 0.1$.

It is observed in the results below that, due to the absence of applied pressure gradients, the contribution of the solution velocity u to the values of $\langle j \rangle$ and ΔV is not crucial in most cases. Thus, the discussion of the results often neglects convection. In general terms, it can be said that the effect of the velocity u on $\langle j \rangle$ and ΔV is equivalent to decreasing the concentration difference between the bulk solutions, since d ln C/dx and dP/dx have opposite signs (see eqs 20a, 20b, 22a, 22b, and 47).

1. Axial and Radial Profiles of Concentration, Potential, and Pressure. Figures 2 and 3 show the axial distributions of the concentration $C(x)$ and the effective pressure $P(x)$ calculated from eqs 49 and 50 for the concentration ratios $c_I/c_{II} = 0.5$ and 5.0 and $c_{II}/X = 0.1$ and 0.5. Actually, the magnitude represented in the pressure distribution is $(P - p_I)/|\Delta\Pi|$, where $\Delta\Pi = 2RT(c_{II} - c_I)$ is the Van't Hoff osmotic pressure difference for point ions. Note that $\Delta P \equiv P(L) - P(0)$ is larger for finite-size than for point ions because $g^* \geq 1$ and $\Delta\Pi^* \geq \Delta\Pi$ (see eq 5). In fact, it can be deduced from eqs 22a and 22b that $\Delta P/\Delta\Pi \approx -[1 + \upsilon(c_I + c_{II})]$. Moreover, it is clearly observed from Figures 2 and 3 that $[C(L) - C(0)]/(c_{II} - c_I) > 1$, and hence, $|dC/dx|$ is larger for finite-size than for point ions. This is a direct consequence of eqs 20a and 20b which is of relevance to the discussion of the solute flux below.

Figures 4 and 5 show the radial distributions of the ionic concentrations, electric potential, and pressure (all in dimensionless form) across the pore section at the axial positions $x = 0$ and $x = L$ for the concentration ratios $c_I/c_{II} = 5.0$ and $c_{II}/X = 0.1$. The ionic concentration distributions clearly show that $\langle c_- \rangle$ is larger for point ions than for finite-size ions. Obviously, $\langle c_+ \rangle = X + \langle c_- \rangle$ is also larger for point ions than for finite-size ions. This means that the effect of ion size is to increase the membrane permselectivity due to the enhanced co-ion exclusion.

The radial distribution of the electric potential ϕ shows the expected behavior. Since the charge density σ at the pore wall is negative, the electric potential is also negative and increases

in magnitude as the pore wall is approached. The ion size effects increase the magnitude of the electrochemical potential $\tilde{\mu}_i$ of co-ions and counterions. Since the conditions of electroneutrality $\langle c_+\rangle = X + \langle c_-\rangle$ and the Donnan equilibria at the membrane|solution interfaces have to be fulfilled, the electric potential must be more negative for finite-size ions than for point ions, as can be observed in Figures 4c and 5c. Finally, the comparison of the electric potential distributions for, for example, point ions in Figures 4c and 5c show that the potential is more negative at $x = L$ than at $x = 0$. This results from the fact that the diffusion potential gradient, which is the main contribution to $\partial\phi/\partial x$ in this case, is negative when $c_I/c_{II} = 5.0$ and $D_- > D_+$.

The radial distribution of pressure shows that it increases in the vicinity of the pore wall, which is a consequence of the fact that the total ionic concentration (and hence the osmotic pressure) is larger there than that at the pore axis. It is clearly seen, for example from Figure 4d, that the pressure at a given location is much larger for finite-size ions than for point ions. This is obviously a result of the excluded volume of finite-size ions and is responsible for the decrease in both $\langle c_-\rangle$ and $\langle c_+\rangle$ with increasing ion size. When comparing Figures 4d and 5d, it is observed that $p(r,L) > p(r,0)$ for both finite-size and point ions. At first, this fact might seem surprising because $p_I = p_{II}$ and $\Pi^*(r,L) < \Pi^*(r,0)$ when $c_I > c_{II}$. However, this results from the fact that the interfacial pressure difference is $\Delta_D p = \Delta_D\Pi^*$ and $\Delta_D\Pi^*(r,L) > \Delta_D\Pi^*(r,0)$. This interfacial osmotic pressure difference is a measure of the different total ion concentration at both sides of the interface and has its origin in the need to compensate the membrane fixed charge. Thus, $\Delta_D\Pi^*$ is larger when the ratio of membrane fixed charge to external electrolyte concentration is larger, and this occurs at $x = L$ when $c_I > c_{II}$.

2. Solute Flux. Figure 6 shows the average solute flux density $\langle j\rangle$ for $c_{II}/X = 0.1$ and 0.5 and for point and finite-size ions. The same flux density values have been plotted against the activity ratio $\gamma_I^* c_I/\gamma_{II}^* c_{II}$ in Figure 6a and b and against the concentration ratio c_I/c_{II} in Figure 6c and d. As expected, the absolute value of $\langle j\rangle$ is smaller for finite-size than for point ions, and $\langle j\rangle$ is negative in the region $\gamma_I^* c_I/\gamma_{II}^* c_{II} < 1$ and positive in the region $\gamma_I^* c_I/\gamma_{II}^* c_{II} > 1$. Note that the shape of the curves is due to the logarithmic scale employed on the abscissa axes.

From eqs 28 and 54, the average solute flux can be expressed as

$$\langle j\rangle = \frac{D_+\langle c_+\rangle\langle c_- u\rangle + D_-\langle c_-\rangle\langle c_+ u\rangle}{D_+\langle c_+\rangle + D_-\langle c_-\rangle} - \frac{2D_+D_-\langle c_+\rangle\langle c_-\rangle}{D_+\langle c_+\rangle + D_-\langle c_-\rangle}\frac{\mathrm{d}\ln C}{\mathrm{d}x} \tag{55}$$

where the first term can be neglected for the present discussion. In the range $\langle c_-\rangle < X$ the coefficient of the second term, $2D_+D_-\langle c_+\rangle\langle c_-\rangle/(D_+\langle c_+\rangle + D_-\langle c_-\rangle)$, is a monotonic function of $\langle c_-\rangle$ that decreases when $\langle c_-\rangle$ does. In the limit of highly charged membranes, $\langle c_-\rangle \ll \langle c_+\rangle \approx X$ and the solute flux density can be approximated by

$$\langle j\rangle \approx -D_- \frac{\mathrm{d}\langle c_-\rangle}{\mathrm{d}x} \tag{56}$$

The ion size effects act to decrease $\langle c_-\rangle$, as shown in Figures 4 and 5, and hence eq 56 explains why $\langle j\rangle$ is smaller for finite-size than for point ions in Figure 6a and b. Note, however, that a paradoxical crossing of the curves for finite-size ions (with no Renkin correction) and for point ions appears in Figure 6d due to the fact that the concentration ratio is used in the abscissa axis, while the activity difference between the bulk solutions is the actual driving force for solute transport.

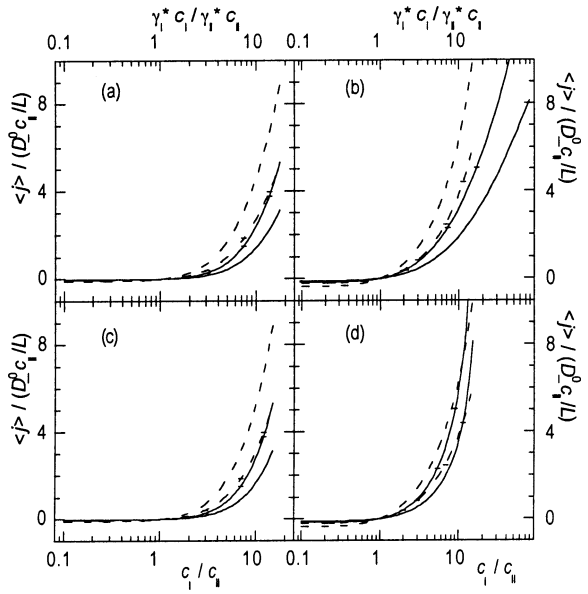

Figure 6. Average solute flux density $\langle j\rangle$ against the activity ratio $\gamma_I^* c_I/\gamma_{II}^* c_{II}$ (plots a and b) and against the concentration ratio c_I/c_{II} (plots c and d) for $c_{II}/X = 0.1$ (plots a and c) and 0.5 (plots b and d). The flux density $\langle j\rangle$ has been normalized to $D^\circ_- c_{II}/L$. Solid curves correspond to finite-size ions of $a_i/a = 0.2$ whose diffusion coefficients D_i have been modified according to the Renkin relation, eq 29; solid curves marked with hyphens (−) correspond to finite-size ions of $a_i/a = 0.2$ with unmodified diffusion coefficients D_i^o; dashed curves correspond to point ions; and dashed curves marked with hyphens (−) correspond to point ions whose diffusion coefficients D_i have been modified according to the Renkin relation for $a_i/a = 0.2$.

Although it is obvious that $\langle j\rangle$ must be smaller for finite-size than for point ions, it is important to know how much of the decrease in the solute flux is due to the fact that the diffusion coefficients D_i have been modified according to the Renkin relation, eq 29, and which is the contribution of the modification of the transport equations of the SCM. So far, when ion size effects were to be taken into account, the results obtained from the SCM for point ions would be modified according to the Renkin relation. This effect is shown in Figure 6 by comparing the two types of dashed curves. It is stressed, however, in the present work that this procedure would account only for a fraction of the ion size effects. The comparison of the solid and dashed curves in Figure 6 marked with hyphens (−) shows that the contribution associated with the modification of the transport equations in the SCM is in fact larger than that due to the Renkin correction. The consideration of both the Renkin relation and the modification of the SCM yields the results shown by the solid lines (with no marks) and shows the practical importance of this correction.

The ion size effects are also analyzed in Figure 8a, which shows the variation of $\langle j\rangle$ with the ratio a_i/a for the case $c_I/c_{II} = 5$ and two values of the ratio c_{II}/X. The curves corresponding to $c_{II}/X = 0.1$ and 0.5 show clearly the decrease of $\langle j\rangle$ with the ion size.

3. Membrane Potential. Parts a and b of Figure 7 show the dependence of the membrane potential on the concentration ratio c_I/c_{II} for both point and finite-size ions. In the region $c_I < c_{II} < X$, the Nernstian slope $\Delta V = \ln(c_I/c_{II})$ of 60 mV/decade is observed, as should be expected in the case of highly charged membranes. In the region $c_I/c_{II} > 1$ the membrane potential

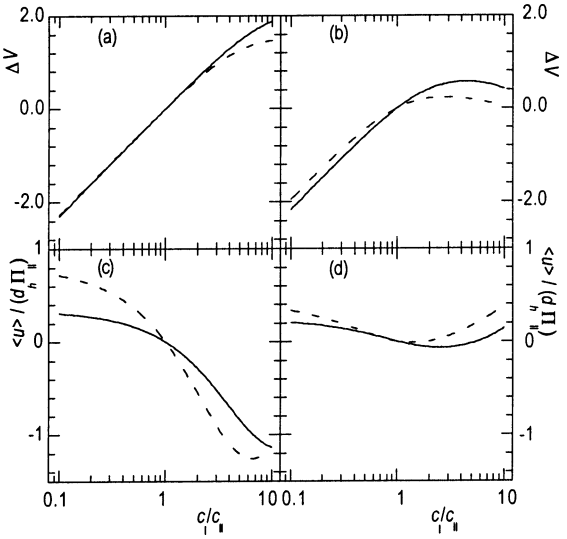

Figure 7. Membrane potential ΔV and average solution velocity $\langle u\rangle$ against the concentration ratio c_I/c_{II} for $c_{II}/X = 0.1$ (plots a and c) and 0.5 (plots b and d). The membrane potential ΔV is in RT/F units, and the solution velocity $\langle u\rangle$ is normalized to $d_h\Pi_{II}$, where $d_h \equiv a^2/8\eta L$ and $\Pi_{II} = 2RTc_{II}$.

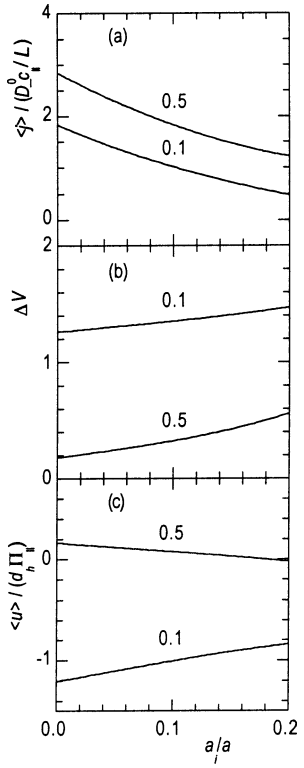

Figure 8. Average solute flux density $\langle j\rangle$, membrane potential ΔV, and average solution velocity $\langle u\rangle$ against the radii ratio a_i/a for $c_I/c_{II} = 5$. The two curves correspond to the cases $c_{II}/X = 0.1$ and 0.5.

shows a maximum (particularly, in the curves corresponding to $c_{II}/X = 0.5$) and tends toward the diffusion potential

$$\Delta V = -\frac{D_- - D_+}{D_- + D_+}\ln\frac{c_I}{c_{II}} \qquad (57)$$

which is negative in this case because $D_- > D_+$.

The full description of the curves shown in Figure 7a and b requires, however, a more detailed analysis. A simple starting point is the equation for the membrane potential derived in the TMS theory (for ideal solutions, point ions, and no convection)

$$\Delta V \approx \ln\frac{([1+4(c_I/X)^2]^{1/2}-1)c_{II}}{([1+4(c_{II}/X)^2]^{1/2}-1)c_I} - \frac{D_- - D_+}{D_- + D_+}\ln\frac{[1+4(c_I/X)^2]^{1/2}+1-2t_-}{[1+4(c_{II}/X)^2]^{1/2}+1-2t_-} \qquad (58)$$

where $t_- \equiv D_-/(D_+ + D_-)$. This equation can also be obtained from the present theoretical approach by introducing approximations such as $\langle c_i\, \partial\phi/\partial x\rangle \approx \langle c_i\rangle\, \mathrm{d}\langle\phi\rangle/\mathrm{d}x$ and $\langle e^{\psi}\rangle \approx e^{\langle\psi\rangle}$. Equation 58 can be used to explain the dashed lines in Figure 7a and b and the two limiting cases above-mentioned.

The solid lines in Figure 7a and b correspond to finite-size ions and show that the absolute value of the membrane potential increases due to ion size effects. Since convection is relatively small (because of the condition $p_I = p_{II}$), eq 54 can be simplified to $\mathrm{d}V/\mathrm{d}x \approx -\sum_i z_i D_i\langle c_i\rangle/(\sum_i D_i\langle c_i\rangle)\ \mathrm{d}\ln C/\mathrm{d}x$. It turns out to be that ion size effects increase both the coefficient $\sum_i z_i D_i\langle c_i\rangle/(\sum_i D_i\langle c_i\rangle)$, because of the enhanced co-ion exclusion shown in Figures 4 and 5, and the gradient $|\mathrm{d}\ln C/\mathrm{d}x|$, as shown in Figures 2 and 3.

The ion size effects can be better analyzed in Figure 8b, which shows the variation of the membrane potential ΔV with the ratio a_i/a for $c_I/c_{II} = 5$ and two values of the ratio c_{II}/X, 0.1 and 0.5. It is clearly shown in this figure that the (absolute value of the) membrane potential increases with the ion size. The intercepts at the origin, that is the membrane potential for point ions, can be calculated from eq 58 as 0.188 and 1.280, in good agreement with the values calculated from the SCM. Finally, the slopes of the curves of ΔV versus a_i/a can be explained from the equation $\mathrm{d}V/\mathrm{d}x \approx -\sum_i z_i D_i\langle c_i\rangle/(\sum_i D_i\langle c_i\rangle)\ \mathrm{d}\ln C/\mathrm{d}x$ and the fact that an increase in a_i/a leads to a decrease in $\langle c_-\rangle$ and an increase in the coefficient $\sum_i z_i D_i\langle c_i\rangle/(\sum_i D_i\langle c_i\rangle)$.

4. Solution Velocity. So far, the discussion of Figures 6a, 7b, and 8a and b has not invoked the convective velocity u. However, the actual values of the solute flux and the membrane potential, and the full comprehension of the trends observed in these figures when varying, for example, the ratio a_i/a, require the consideration of the solution velocity. Parts c and d of Figure 7 show the average velocity $\langle u\rangle$ against the concentration ratio c_I/c_{II} for the cases $c_{II}/X = 0.1$ and 0.5. In these figures, the solution velocity $\langle u\rangle$ has been normalized to $d_h\Pi_{II}$, where $d_h \equiv a^2/8\eta L$ and $\Pi_{II} = 2RTc_{II}$. Obviously, $\langle u\rangle = 0$ when $c_I = c_{II}$. In the case of Figure 7c ($c_{II}/X = 0.1$), the average solution velocity for both point and finite-size ions shows the behavior that could be expected from the osmotic pressure difference between the external solutions; that is, the solution flows from the lower to the higher external concentration. However, when $c_{II}/X = 0.5$ and c_I/c_{II} is larger than $\sim$2 in the case of point ions and $\sim$6 in the case of finite-size ions, Figure 7d shows that the solution velocity reverses sign and the anomalous negative osmosis effect is evidenced.[16]

Besides the osmotic pressure difference between the external solutions, there is also an electric force acting on the solution filling the pores. This force is the product of the space charge density $\rho_e \equiv F\Sigma_i z_i c_i > 0$ and the axial electric field $-\partial\Phi/\partial x$ inside the membrane. The axial electric field is mainly due to the diffusion potential, and it is positive when $c_I > c_{II}$ and negative otherwise, as can be deduced from eq 58 and the condition $D_- > D_+$. Therefore, the electric force acting on the solution moves the solution toward the external solution of lower concentration. That is, electric and osmotic forces act in opposite

directions. In the case of highly charged membranes, the magnitude of the diffusion potential is very small and the osmotic pressure difference $\Delta\Pi$ determines the sign of the convective velocity, as shown in Figure 7c. When X decreases, the force acting on the solution filling the pore also decreases because the electric and osmotic forces tend to cancel out; the net force and the mass-average velocity $\langle u\rangle$ vanish in the case of neutral membranes and $p_I = p_{II}$.[16] This suggests that the absolute value of $\langle u\rangle$ must decrease when c_{II}/X increases, as can be observed from the comparison of Figure 7c and d. The electric force, however, does not show a monotonic behavior with varying X, and hence, it happens sometimes that the electric force becomes larger than the osmotic one and the anomalous negative osmotic effect becomes so pronounced that $\langle u\rangle$ reverses direction.

Figure 8c shows the variation of $\langle u\rangle$ with the ratio a_i/a for the case $c_I/c_{II} = 5$ and the values of the ratio c_{II}/X considered in Figure 7c and d. In both cases, the absolute value of the convective velocity $\langle u\rangle$ decreases with increasing ion size. If this decrease were to be ascribed to the fact that the average velocity $\langle u\rangle$ is roughly proportional to a^{*2}, the variation of $\langle u\rangle$ with a_i/a would follow the simple relation $\langle u\rangle(a_i)/\langle u\rangle(0) \approx (1 - a_i/a)^2$. This relation is roughly in agreement with the curve corresponding to $c_{II}/X = 0.1$, at least up to $a_i/a = 0.1$, but it underestimates the variation observed in the curve corresponding to $c_{II}/X = 0.5$. This implies that ion size also affects the values of the osmotic and electric forces acting on the pore solution and hence the observed convective velocity.

IV. Conclusions

The SCM has been extended to account for the finite size of the ions and solvent molecules. The corresponding equation system has been solved to study the electrokinetic flow in nanoporous membranes caused by concentration gradients. One of the fundamental consequences of incorporating ion size effects is that the average ionic concentrations in the pore solution decrease, while satisfying the global electroneutrality condition $\langle c_+\rangle = X + \langle c_-\rangle$. The membrane shows then an enhanced co-ion exclusion and behaves in some aspects as having an effective fixed charge concentration larger than X.

In a highly charged membrane the solute flux density is roughly equal to the co-ion flux density, and therefore, the ion size effects act to decrease the absolute value of the pore-average solute flux density $\langle j\rangle$. In other words, the membrane exhibits a significantly lower permeability than that expected for point ions and the decrease in permeability cannot be simply taken into account through the Renkin relation. Thus, it is concluded that this extension of the SCM should be used, at least, when analyzing permeability measurements.

Another consequence of the enhanced co-ion exclusion is that the absolute value of the membrane potential increases with the ion size. This increase is of minor importance in the region $c_I < c_{II} < X$, where the membrane potential exhibits the Nernstian slope $\Delta V = \ln(c_I/c_{II})$, but becomes more pronounced at larger concentrations.

At low electrolyte concentrations, the solution flows from the lower to the higher external concentration, as could be expected from the normal osmotic behavior. At high concentrations, however, the anomalous negative osmosis effect can appear. In any case, the absolute value of the average solution velocity decreases with increasing ion size. This is partly due to the reduction of the effective pore radius $a^* \equiv a - a_i$, but the finite ion size also affects the values of the osmotic and electric forces acting on the pore solution. These results, together with those presented in refs 57 and 58, constitute a sound theoretical framework which allows the study of flow in nanoporous membranes driven by electric current, pressure differences, and concentration differences.

Acknowledgment. Financial support from the Ministry of Science and Tecnology of Spain and the Fondo Europeo de Desarrollo Regional (FEDER) under Project No. MAT2002-00646 is gratefully acknowledged. Helpful discussions with Profs. S. Mafé and J. A. Manzanares are also acknowledged.

References and Notes

(1) Verbrugge, M. W.; Pintauro, P. N. In *Modern Aspects of Electrochemistry*; Conway, B. E., Bockris, J. O'M., White, R. E., Eds.; Plenum Press: New York, 1989; Vol. 19, pp 1−67.
(2) Lakshminarayanaiah, N. *Equations of Membrane Biophysics*; Academic Press: New York, 1984.
(3) Teorell, T. *Proc. Soc. Exp. Biol. Med.* **1935**, *33*, 282−285.
(4) Meyer, H.; Sievers, J. F. *Helv. Chim. Acta* **1936**, *19*, 649−664.
(5) Morrison, F. A.; Osterle, J. F. *J. Chem. Phys.* **1965**, *43*, 2111−2115.
(6) Gross, R. J.; Osterle, J. F. *J. Chem. Phys.* **1968**, *49*, 228−234.
(7) Fair, J. C.; Osterle, J. F. *J. Chem. Phys.* **1971**, *54*, 3307−3316.
(8) Kobatake, Y. *J. Chem. Phys.* **1958**, *28*, 146−153.
(9) Dresner, L.; Kraus, K. A. *J. Phys. Chem.* **1963**, *67*, 990−996.
(10) Dresner, L. *J. Phys. Chem.* **1963**, *67*, 1635−1641.
(11) Dresner, L. *J. Phys. Chem.* **1965**, *69*, 2230−2238.
(12) Westermann-Clark, G. B.; Christoforou, C. C. *J. Electroanal. Chem.* **1986**, *198*, 213−231.
(13) Koh, W. H.; Silverman, H. P. *J. Membr. Sci.* **1983**, *13*, 279−290.
(14) Westermann-Clark, G. B.; Anderson, J. L. In *Ion Exchange: Transport and Interfacial Properties*; Yeo, R. S., Buck, R. P., Eds.; The Electrochemical Society: Princeton, NJ, 1981; Vols. 81−82, pp 33−45.
(15) Sashidhar, V.; Ruckenstein, E. *J. Colloid Interface Sci.* **1981**, *82*, 439−457.
(16) Sashidhar, V.; Ruckenstein, E. *J. Colloid Interface Sci.* **1982**, *85*, 332−362.
(17) Mafé, S.; Manzanares, J. A.; Pellicer, J. *J. Membr. Sci.* **1990**, *51*, 161−168.
(18) Manzanares, J. A.; Mafé, S.; Pellicer, J. *J. Non-Equilib. Thermodyn.* **1991**, *16*, 255−265.
(19) Aguilella, V. M.; Pellicer, J.; Aguilella-Arzo, M. *Langmuir* **1999**, *15*, 6156−6162.
(20) Martínez, L.; Hernández, A.; González, A.; Tejerina, F. *J. Colloid Interface Sci.* **1992**, *152*, 325−332.
(21) Cwirko, E. H.; Carbonell, R. G. *J. Colloid Interface Sci.* **1989**, *129*, 513−531.
(22) Yang, Y.; Pintauro, P. N. *AIChE J.* **2000**, *46*, 1177−1190.
(23) Cwirko, E. H.; Carbonell, R. G. *J. Membr. Sci.* **1992**, *67*, 227−247.
(24) Pintauro, P. N.; Verbrugge, M. W. *J. Membr. Sci.* **1989**, *44*, 197−212.
(25) Guzmán-García, A. G.; Pintauro, P. N.; Verbrugge, M. W.; Hill, R. F. *AIChE J.* **1990**, *36*, 1061−1074.
(26) Bontha, J. R.; Pintauro, P. N. *Chem. Eng. Sci.* **1994**, *49*, 3835−3851.
(27) Basu, S.; Sharma, M. *J. Membr. Sci.* **1997**, *124*, 77−91.
(28) Borukhov, I.; Andelman, D.; Orland, H. *Phys. Rev. Lett.* **1997**, *79*, 435−438.
(29) Paunov, V. N.; Dimova, R. I.; Kralchevsky, P. A.; Broze, G.; Mehreteab, A. *J. Colloid Interface Sci.* **1996**, *182*, 239−248.
(30) Paunov, V. N.; Binks, B. P. *Langmuir* **1999,** *15*, 2015−2021.
(31) Pade, V.; Stavchansky, S. *Pharm. Res.* **1997**, *14*, 1210−1215.
(32) Cárdenas, A. E.; Coalson, R. D.; Kurnikova, M. G. *Biophys. J.* **2000**, *79*, 80−93.
(33) Eisenberg, R. S. *Acc. Chem. Res.* **1998**, *31*, 5509−5514.
(34) Bikerman, J. *Philos. Mag.* **1942**, *33*, 384−392.
(35) Grimley, T. B.; Mott, N. F. *Discuss. Faraday Soc.* **1947**, *1*, 3−11.
(36) Wicke, E.; Eigen, M. *Z. Elektrochem.* **1953**, *57*, 319−330.
(37) Freise, V. *Z. Elektrochem.* **1952**, *56*, 822−827.
(38) Sparnaay, M. J. *The Electrical Double Layer*; Pergamon Press: Oxford, 1972.
(39) Brodowsky, H.; Strehlow, H. *Z. Elektrochem.* **1959**, *63*, 262−269.
(40) Levine, S.; Bell, G. M. *J. Phys. Chem.* **1960**, *64*, 1188−1195.
(41) Gur, Y.; Ravina, I.; Babchin, A. J. *J. Colloid Interface Sci.* **1978**, *64*, 326−332.

(42) Gonzalez-Tovar, E.; Lozada-Cassou, M.; Olivares, W. *J. Chem. Phys.* **1991**, *94*, 2219−2231.
(43) Renkin, E. M. *J. Gen. Physiol.* **1954**, *38*, 225−243.
(44) Haase, R. *Thermodynamics of Irreversible Processes*; Addison-Wesley: London, 1969.
(45) Buck, R. P. *J. Membr. Sci.* **1984**, *17*, 1−62.
(46) Babchin, A. J.; Frenkel, A. L. *J. Colloid Interface Sci.* **1985**, *106*, 410−421.
(47) Keh, H. J.; Wu, J. H. *Langmuir* **2001**, *17*, 4216−4222.
(48) Kobatake, Y.; Toyoshima, Y.; Takeguchi, N. *J. Phys. Chem.* **1966**, *70*, 1187−1193.
(49) Huerta, M.; Olivares, W. *J. Phys. Chem.* **1987**, *91*, 2975−2978.
(50) Yeomans, L.; Feller, S. E.; Sánchez, E.; Lozada-Cassou, M. *J. Chem. Phys.* **1993**, *98*, 1436−1450.
(51) Mafé, S.; Ramírez, P.; Tanioka, A.; Pellicer, J. *J. Phys. Chem. B* **1997**, *101*, 1851−1856.
(52) Mafé, S.; Ramírez, P.; Manzanares, J. A. *Colloid Polym. Sci.* **1997**, *275*, 599−603.
(53) Mafé, S.; Ramírez, P.; Pellicer, J. *J. Membr. Sci.* **1998**, *138*, 269−277.
(54) Szymcyk, A.; Aoubiza, B.; Fievet, P.; Pagetti, J. *J. Colloid Interface Sci.* **1999**, *216*, 285−296.
(55) Guggenheim, E. A. *Thermodynamics*; North-Holland: Amsterdam, 1967.
(56) Garrido, J.; Manzanares, J. A. *J. Phys. Chem. B* **2000**, *104*, 658−662.
(57) Cervera, J.; Manzanares, J. A.; Mafé, S. *Phys. Chem. Chem. Phys.* **2001**, *3*, 2493−2496.
(58) Cervera, J.; Manzanares, J. A.; Mafé, S. *J. Membr. Sci.* **2001**, *191*, 179−187.
(59) Manzanares, J. A.; Mafé, S.; Bisquert, J. *Ber. Bunsen-Ges. Phys. Chem.* **1992**, *96*, 538−544.
(60) Sims, S. M.; Higuchi, W. I.; Srinivasan, V.; Peck, K. *J. Colloid Interface Sci.* **1993**, *155*, 210−220.
(61) Press, W. H.; Flannery, B. P.; Teukolsky, S. A.; Vetterling, W. T. *Numerical Recipes*; Cambridge University Press: Cambridge, 1988.